DRAFT VERSION FEBRUARY 3, 2006
Preprint typeset using LaTeX style emulateapj v. 6/22/04



# MEASURING THE THREE-DIMENSIONAL STRUCTURE OF GALAXY CLUSTERS. II. ARE CLUSTERS OF GALAXIES OBLATE OR PROLATE?

MAURO SERENO[1,2,3,4], ELISABETTA DE FILIPPIS[1,2,5], GIUSEPPE LONGO[1,2,3], AND MARK W.BAUTZ[5]

(Dated:)
*Draft version February 3, 2006*

## ABSTRACT

The intrinsic shape of galaxy clusters can be obtained through a combination of X-ray and Sunyaev-Zeldovich effect observations once cosmological parameters are assumed to be known. In this paper we discuss the feasibility of modelling galaxy clusters as either prolate or oblate ellipsoids. We analyze the intra-cluster medium distribution for a sample of $25$ X-ray selected clusters, with measured Sunyaev-Zeldovich temperature decrements. A mixed population of prolate and oblate ellipsoids of revolution fits the data well, with prolate shapes preferred on a $\sim 60-76\%$ basis. We observe an excess of clusters nearly aligned along the line of sight, with respect to what is expected from a randomly oriented cluster population, which might imply the presence of a selection bias in our sample. We also find signs that a more general triaxial morphology might better describe the morphology of galaxy clusters. Additional constraints from gravitational lensing could disentangle the degeneracy between an ellipsoidal and a triaxial morphology, and could also allow an unbiased determination of the Hubble constant.

*Subject headings:* Galaxies: clusters: general – X-rays: galaxies: clusters – cosmology: observations – distance scale – gravitational lensing – cosmic microwave background

## 1. INTRODUCTION

Measuring the three-dimensional shape of any class of astronomical object is today still an almost unsolved task which has challenged astronomers for decades. The knowledge of the shape of clusters of galaxies in particular has fundamental cosmological implications. In a cold dark matter scenario, smaller clumps aggregate hierarchically along large-scale perturbations, which are typically highly anisotropic at their first collapse. Accretion of material might hence preferentially occur along the filamentary structure within which larger matter aggregates (i.e. galaxy clusters) are embedded (West 1994). This could explain the observed tendency of clusters to be aligned with their nearest neighbor (Carter & Metcalfe 1980). Further processes, such as virialization of the matter aggregates or self-interaction mechanisms for dark matter, might on the other hand tend to make such systems more spherical. Dissipation and gas cooling could result in an average increase of the axis ratios of dark matter halos by $\sim 20-40\%$ in the inner regions, with effects persisting almost to the virial radius (Kazantzidis et al. 2004). The intrinsic shape of structures therefore contains evidence of the formation history of the large-scale structure and about the nature and mechanisms of interaction of dark matter (Plionis et al. 1991, 2004, and references therein).

The first attempts to determine the three dimensional morphology of galaxies with only photometric data (Binney & Merrifield 1998, and references therein) led to the realization that since objects might be either triaxial or build up a mixture of oblate and prolate shapes, a purely geometrical and statistical analysis will not produce a unique solution (Binggeli 1980).

First results came from the original work of Hubble (1926), who first determined the relative frequencies with which galaxies of a given intrinsic ellipticity, oriented at random, will be observed as having various apparent projected ellipticities. Several studies have subsequently generalized Hubble's work (Binney & Merrifield 1998, and references therein), making the statistical approach of inversion of the distribution of the apparent shapes of galaxies a widely used method. This inversion method has several drawbacks, though. First of all, it is not unambiguous since it requires strong assumptions on the distribution of the intrinsic shapes of the structures. The distribution of the apparent flattening is moreover rather insensitive to modifications in the model assumed for the intrinsic shapes (Binggeli 1980); different distributions of oblate or prolate spheroids, or generally triaxial ellipsoids, can consequently be consistent with the observed distribution of axial ratios. Simplifying hypotheses, such as requiring structures to be oblate, can hence be strongly misleading (Bertola & Capaccioli 1975; Illingworth 1977); for a more correct approach, prolate and triaxial models should also be considered.

While the first investigation by Hubble (1926) was done on galaxies, several following studies have faced the inversion method for different classes of astronomical objects such as poor groups or clusters of galaxies (Binney & de Vaucouleurs 1981; Thakur & Chakraborty 2001; Fasano & Vio 1991; Noerdlinger 1979; Alam & Ryden 2002; Binggeli 1980; Ryden 1992, 1996; Plionis et al. 2004). With the exception of disc galaxies, prolate-like shapes appear to dominate all cosmic structure on a large scale (Plionis et al. 2004).

In this paper, we are interested in obtaining the three-dimensional shape of clusters of galaxies. So far, studies on clusters have been limited to the statistical inversion of the apparent distribution of axial ratios. Plionis et al. (1991) found that the distribution of apparent axial ratios of 397 Abell clus-

[1] Dipartimento di Scienze Fisiche, Università degli Studi di Napoli 'Federico II', Via Cinthia, Compl. Univ. Monte S. Angelo, 80126 Napoli, Italia
[2] INFN - Sez. Napoli, Compl. Univ. Monte S. Angelo, 80126 Napoli, Italia; betty@na.infn.it; longo@na.infn.it
[3] INAF - Osservatorio Astronomico di Capodimonte, Salita Moiariello, 16, 80131 Napoli, Italia
[4] Institut für Theoretische Physik, Universität Zürich, Winterthurerstrasse 190, CH-8057 Zürich, Schweiz; sereno@physik.unizh.ch
[5] Massachusetts Institute of Technology, Kavli Center for Astrophysics and Space Research, Building 37, Cambridge MA 02139 USA; mwb@space.mit.edu

ters, selected from the Lick map of galaxies, is inconsistent with a population of oblate spheroids. Similar results are reported by Basilakos et al. (2000) and de Theije et al. (1995), who find that a population composed by purely prolate spheroids is more consistent with, respectively, a sample of 903 clusters from the APM catalog and with a set of 99 low redshift Abell clusters, better than a purely oblate population. While the above studies were performed uniquely on optical data, Cooray (2000) used the X-ray isophotal axial ratios of a sample of 58 clusters by Mohr et al. (1995); a population of purely oblate ellipsoids is again ruled out. A quite different approach was followed in Paz et al. (2006), where observational data from 2PIGG and SDSS group catalogues were compared to projected shapes of numerically simulated haloes. Haloes turned out to be preferentially prolate, with more massive groups tending to show more elongated shapes.

The above listed results are based on the controversial assumption that objects are randomly oriented in space. Furthermore, tests for possible intrinsic triaxial or mixed populations have to date been far from conclusive. Several works in the past few years have discussed how multi-wavelength observations of clusters of galaxies can be used to uncover the 3-D structure of clusters of galaxies (Zaroubi et al. 1998, 2001; Reblinsky 2000; Fox & Pen 2002). In a companion paper (De Filippis et al. 2005) (hereafter, Paper I), we have considered the theoretical capability of combined X-ray, Sunyaev-Zeldovich effect (SZE) and gravitational lensing observations to determine the 3-D morphology of relaxed galaxy clusters and, jointly, to constrain cosmological parameters. Due to a lack of gravitational lensing data, we have then used X-ray and SZE measurements of a sample of 25 clusters to constrain their triaxial structure by assuming the concordance cosmological $\Lambda$CDM model, which is determined to an unprecedented accuracy thanks to an impressive body of evidence coming from several cosmological tests (Wang et al. 2000; Tegmark et al. 2004).

In this paper, we test the accuracy to which ellipsoids of revolution can describe the sample of clusters of galaxies we studied in Paper I. Following a similar empirical approach, we use combined X-ray and SZE observations to directly probe the 3-D structure of clusters in the sample, without any assumptions on their statistical properties. The paper is organized as follows. In § 2 we discuss how the shape of an ellipsoid of revolution can be obtained from combined X-ray and SZE measurements. In § 3 we introduce our cluster sample and derive the intrinsic distributions of the axial ratios and inclination angles for the cluster sample, together with a comparison between these results and those obtained in Paper I assuming a triaxial morphology aligned along the line of sight. In § 4 we perform a statistical inversion of the observed distribution of projected axial ratios. In § 6 some systematics are considered. Further information that can be obtained with additional constraints from gravitational lensing observations is discussed in § 5. § 7 is devoted to conclusions and final considerations. In Appendix A, we provide some mathematical details on the two-dimensional projection of an ellipsoid.

## 2. ELLIPSOIDS OF REVOLUTION

In this paper we assume that galaxy clusters have an axisymmetric gas density distribution. The intrinsic distribution of the intra-cluster medium (ICM), assumed to be constant on similar, concentric spheroidal ellipsoids, is characterized by the ratio of the major to minor axes $e_{\rm int}(>1)$, and by the inclination angle $i$, between the line of sight (LOS) of the observer and the polar axis. In an intrinsic orthogonal coordinate system centred on the cluster's barycentre and whose coordinates are aligned with its principal axes, a spheroidal ICM profile can be described by only one radial variable $\zeta$,

$$\zeta^2 \equiv \sum_{i=1}^{3} e_i^2 x_{i,\rm int}^2. \tag{1}$$

If we take the axis of symmetry aligned with the third coordinate, $e_i = \{e_{\rm int}, e_{\rm int}, 1\}$ for a prolate model and $e_i = \{1, 1, e_{\rm int}\}$ for an oblate model.

For an intrinsic 3-D spheroidal morphology, the two-dimensional observed quantities, projected on the plane of the sky (POS), are constant on concentric ellipses. The axial ratio of the major to minor axes of the observed projected isophotes, $e_{\rm proj}$, can be expressed as a function of the cluster intrinsic parameters (Fabricant et al. 1984),

$$e_{\rm proj} = \begin{cases} \sqrt{\cos^2 i + e_{\rm int}^2 \sin^2 i} & \text{prolate case} \\ \dfrac{e_{\rm int}}{\sqrt{e_{\rm int}^2 \cos^2 i + \sin^2 i}} & \text{oblate case} \end{cases} \tag{2}$$

In Paper I, we discussed how the elongation along the LOS of a cluster of galaxies, $e_{\rm LOS}$, can be determined by combining X-ray and SZE observations if a reliable estimate of the Hubble constant is provided. For a spheroid inclined with respect to the LOS, as we assume clusters to be shaped in this paper, $e_{\rm LOS}$ represents the ratio of the size of the spheroid along the LOS, measured through its barycentre, to the size of the major axis projected in the POS. A value of $e_{\rm LOS}$ greater than one corresponds to a cluster elongated along the LOS, and vice versa for $e_{\rm LOS} < 1$. For the cluster plasma density we assume an isothermal $\beta$-distribution:

$$n_{\rm e}(\zeta) \propto \left(1 + \frac{\zeta^2}{r_{\rm c}^2}\right)^{-3\beta/2}, \tag{3}$$

where $r_{\rm c}$ is the core radius and $\beta$ the slope parameter. For such a distribution, $e_{\rm LOS}$ can then be written as (Paper I):

$$e_{\rm LOS} \equiv \left[\frac{\Delta T_0^2}{S_{\rm X0}} \left(\frac{m_{\rm e}c^2}{k_{\rm B}T_{\rm e}}\right)^2 \frac{\Lambda_{\rm e}\mu_{\rm e}/\mu_{\rm H}}{4\pi^{3/2} f(\nu, T_{\rm e})^2 T_{\rm CMB}^2 \sigma_{\rm T}^2 (1+z_{\rm c})^4} \times \left(\frac{\Gamma[3\beta/2]}{\Gamma[3\beta/2 - 1/2]}\right)^2 \frac{\Gamma[3\beta - 1/2]}{\Gamma[3\beta]} \frac{1}{\theta_{\rm c,proj}}\right] \frac{1}{D_{\rm c}}. \tag{4}$$

where $z$ is the cluster redshift, $D_{\rm c}$ the angular diameter distance to the cluster, $\Delta T_0$ the central SZE temperature decrement, $\theta_{\rm c,proj}$ the projected angular major core radius, $T_{\rm e}$ the temperature of the ICM, $k_{\rm B}$ the Boltzmann constant, $T_{\rm CMB} = 2.728$°K (Fixsen et al. 1996) the temperature of the cosmic microwave background radiation, $\sigma_{\rm T}$ the Thompson cross section, $m_{\rm e}$ the electron mass, $\mu m_{\rm p}$ the mean particle mass of the gas, $c$ the speed of light in vacuum, $\Lambda_e$ the X-ray cooling function of the ICM in the cluster rest frame, $S_{\rm X0}$ the central X-ray surface brightness and $f(\nu, T_{\rm e})$ accounts for frequency shift and relativistic corrections. In a flat Friedmann-Lemaître-Robertson-Walker model of universe filled with dust, $\Omega_{\rm M0}$, and with a non null cosmological constant, the angular diameter distance to a source at a redshift $z$ is (Sereno et al. 2001)

$$D_{\rm c} = \frac{c}{H_0} \frac{1}{1+z} \int_0^z \frac{dx}{\sqrt{\Omega_{\rm M0}(1+x)^3 + 1 - \Omega_{\rm M0}}}. \tag{5}$$

We assume a flat ΛCDM model with a Hubble constant $H_0 = 70^{+4}_{-3}$ km s$^{-1}$Mpc$^{-1}$ and $\Omega_{\rm M0} = 0.30 \pm 0.04$ (Tegmark et al. 2004). As well known, if the Hubble constant is not assumed from independent observational constraints, then the length of a cluster along the LOS can be known from SZE and X-ray observations only up to a multiplicative factor (Cooray 1998). When we use experimental data provided with asymmetric uncertainties, corrections as given by D'Agostini (2004) are applied to obtain unbiased estimates of mean and standard deviation.

In terms of $e_{\rm proj}$ we can also write (De Filippis et al. 2005; Donahue et al. 2003)

$$e_{\rm LOS} = \begin{cases} \dfrac{\sqrt{e^2_{\rm proj} - \cos^2 i}}{e^2_{\rm proj} \sin i} & \text{prolate case} \\ \dfrac{\sqrt{1 - e^2_{\rm proj} \cos^2 i}}{\sin i} & \text{oblate case} \end{cases} \quad (6)$$

For clusters aligned along the LOS (i.e. $i = 0$) both prolate and oblate distributions exhibit circular isophotes and $e_{\rm LOS}$ can be expressed as a function of the cluster intrinsic ellipticity as follows:

$$e_{\rm LOS} = \begin{cases} e_{\rm int} & \text{prolate case} \\ \dfrac{1}{e_{\rm int}} & \text{oblate case.} \end{cases} \quad (7)$$

If we assume the cluster to be either prolate or oblate Eqs. (2, 6), enable us to determine the intrinsic geometry of the cluster. In the prolate case, we obtain

$$e_{\rm int} = e_{\rm LOS} e^2_{\rm proj}; \quad (8)$$

$$i = \pm \arccos \left[ \sqrt{\frac{e^2_{\rm int} - e^2_{\rm proj}}{e^2_{\rm int} - 1}} \right], \quad (9)$$

while in the oblate case:

$$e_{\rm int} = \frac{e_{\rm proj}}{e_{\rm LOS}} \quad (10)$$

$$i = \pm \arccos \left[ \sqrt{\frac{e^2_{\rm LOS} - 1}{e^2_{\rm LOS} - e^2_{\rm proj}}} \right]. \quad (11)$$

We are dealing with observed projected quantities which are invariant under a reflection through the POS. Hence we are not able to determine which extremity of the cluster is pointing towards the observer.

## 3. INTRINSIC DISTRIBUTIONS THROUGH COMBINED X-RAY AND SZE MEASUREMENTS

In this section, we apply the formalism described in § 2 to compute the three-dimensional intrinsic elongation and inclination for the same cluster sample used in Paper I, for which a combined X-ray and SZE data set was available. The sample consists of 25 clusters of galaxies, 18 from Reese et al. (2002) and 7 from Mason et al. (2001). Details on the sample and on the selection criteria can be found in Mason et al. (2001); Reese et al. (2002); De Filippis et al. (2005). Basic data for our 25 clusters, including previously published redshift, plasma temperature and SZE decrement information are presented in Table 1 of Paper I. In Paper I, we also measured projected axial ratios, $e_{\rm proj}$, for all clusters in the sample through an X-ray morphological analysis based on high resolution *Chandra* and *XMM-Newton* observations; measured values are listed in Table 2 of Paper I.

Through a combined analysis of both X-ray and SZE observations, we can infer new information about intrinsic elongation and inclination of the clusters in the sample. We then model these distributions with a kernel empirical estimator (Vio et al. 1994; Ryden 1996). Given a sample of $N$ measured quantities $\eta_i$, the kernel estimator of the distribution is a continuous function given by:

$$N_\eta(\eta) = \frac{1}{Nh} \sum_{i=1}^{N} K\left(\frac{\eta - \eta_i}{h}\right) \quad (12)$$

where $K$ is the kernel function. When densities take values in the range $0 \le \eta \le \eta_{\rm max}$, the kernel can be written as:

$$K_{\rm ref}(\eta, \eta_i, h) = K_{\rm Gau}\left(\frac{\eta - \eta_i}{h}\right) + K_{\rm Gau}\left(\frac{\eta + \eta_i}{h}\right) + K_{\rm Gau}\left(\frac{2\eta_{\rm max} - \eta - \eta_i}{h}\right) \quad (13)$$

where $K_{\rm Gau}$ is a Gaussian kernel given by:

$$K_{\rm Gau}(x) = \frac{1}{\sqrt{2\pi}} e^{-x^2/2}. \quad (14)$$

When using the kernel in Eq. (13), Gaussian tails extending to negative values or to values greater than $\eta_{\rm max}$, are folded back between 0 and $\eta_{\rm max}$. The kernel width $h$ can be approximated by $h \simeq 0.9AN^{-0.2}$, where $A$ is the smallest quantity between the standard deviation of the sample and the interquartile range divided by 1.34 (Vio et al. 1994).

In order to account for the effect of the finite sample size, we derive the confidence levels from a bootstrap re-sampling of the data set. From the distribution obtained with the original $N$ data points, we draw with replacement a new set of $N$ data points which are then used to create a new bootstrap estimate of the kernel estimator, $N_\eta$. Confidence intervals can then be assigned to each value of $\eta$, by finding the values of $N_\eta$ that lie above (below) the required upper (lower) confidence limit. Errors in the measured value of $\eta$ induce a further uncertainty in the estimated distribution. This effect can be modelled with a kernel width given by:

$$h_i' = \sqrt{h^2 + \Delta\eta_i^2} \quad (15)$$

which changes for each data point (Ryden 1996).

In what follows, we use the inverse of the intrinsic and projected axial ratios: $q_{\rm int} \equiv 1/e_{\rm int}$ and $q_{\rm proj} \equiv 1/e_{\rm proj}$. Such a formalism allows axial ratios to be limited to the finite range $(0, 1]$. The histogram in Fig. 1 represents the observed distribution of the projected axial ratios. Confidence limits are built up with $10^3$ bootstrap re-samplings. Estimates of the observed projected ellipticity from both *Chandra* and *XMM-Newton* satellites are so accurate that for the distribution of observed axial ratios $h_i' \simeq h$. The measured mean ellipticity is $q_{\rm proj} = 0.80 \pm 0.02$; the value of the median is instead 0.81. Reported uncertainties represent the standard deviation of the mean. These values are in good agreement with the average projected axial ratio expected if dark matter halos of clusters do have mass distributions as revealed by numerical simulations (Wang & Fan 2004). The solid and the dashed lines in Fig. 1 show the non-parametric kernel estimate and the 2-$\sigma$ confidence range, respectively, using the bootstrap procedure.

### 3.1. *Axial ratios*

TABLE 1
INTRINSIC PARAMETERS OF SAMPLE CLUSTERS

| Cluster | $z$ | Shape | $q_{\rm int}$ (ellips.) | $i$ (deg) | $q_{\rm int}$ (triax.) |
|---|---|---|---|---|---|
| MS 1137.5+6625 | 0.784 | pro | $0.49 \pm 0.21$ | $16 \pm 9$ | $0.56 \pm 0.21$ |
| MS 0451.6-0305 | 0.550 | obl | $0.71 \pm 0.16$ | $58 \pm 43$ | $0.76 \pm 0.06$ |
| – | – | pro | $0.63 \pm 0.14$ | $56 \pm 13$ | – |
| Cl 0016+1609 [a] | 0.546 | pro | $0.55 \pm 0.13$ | $26 \pm 10$ | $0.67 \pm 0.14$ |
| RXJ1347.5-1145 [a] | 0.451 | obl | $0.68 \pm 0.16$ | $84 \pm 117$ | $0.69 \pm 0.09$ |
| – | – | pro | $0.48 \pm 0.11$ | $35 \pm 12$ | – |
| A 370 | 0.374 | pro | $0.35 \pm 0.13$ | $27 \pm 12$ | $0.55 \pm 0.15$ |
| MS 1358.4+6245 [a] | 0.327 | obl | $0.55 \pm 0.14$ | $52 \pm 8$ | $0.71 \pm 0.06$ |
| A 1995 | 0.322 | obl | $0.75 \pm 0.18$ | $64 \pm 35$ | $0.81 \pm 0.09$ |
| – | – | pro | $0.70 \pm 0.16$ | $46 \pm 27$ | – |
| A 611 | 0.288 | pro | $0.73 \pm 0.26$ | $35 \pm 32$ | $0.84 \pm 0.19$ |
| A 697 | 0.282 | pro | $0.44 \pm 0.12$ | $26 \pm 10$ | $0.60 \pm 0.14$ |
| A 1835 [a] | 0.252 | pro | $0.56 \pm 0.08$ | $29 \pm 7$ | $0.70 \pm 0.09$ |
| A 2261 [a] | 0.224 | pro | $0.63 \pm 0.16$ | $10 \pm 6$ | $0.65 \pm 0.16$ |
| A 773 | 0.216 | pro | $0.32 \pm 0.09$ | $14 \pm 5$ | $0.40 \pm 0.11$ |
| A 2163 [a] | 0.202 | pro | $0.62 \pm 0.13$ | $28 \pm 10$ | $0.73 \pm 0.12$ |
| A 520 | 0.202 | obl | $0.54 \pm 0.20$ | $23 \pm 10$ | $0.56 \pm 0.08$ |
| A 1689 [a] | 0.183 | obl | $0.85 \pm 0.12$ | $65 \pm 44$ | $0.88 \pm 0.06$ |
| – | – | pro | $0.79 \pm 0.11$ | $46 \pm 23$ | – |
| A 665 | 0.182 | obl | $0.58 \pm 0.25$ | $47 \pm 13$ | $0.71 \pm 0.15$ |
| A 2218 | 0.171 | pro | $0.54 \pm 0.18$ | $22 \pm 11$ | $0.64 \pm 0.18$ |
| A 1413 [a] | 0.142 | obl | $0.64 \pm 0.17$ | $73 \pm 33$ | $0.68 \pm 0.09$ |
| – | – | pro | $0.49 \pm 0.13$ | $37 \pm 15$ | – |
| A 2142 [a] | 0.091 | obl | $0.63 \pm 0.13$ | $79 \pm 42$ | $0.65 \pm 0.07$ |
| – | – | pro | $0.43 \pm 0.09$ | $34 \pm 10$ | – |
| A 478 [a] | 0.088 | pro | $0.34 \pm 0.14$ | $23 \pm 12$ | $0.51 \pm 0.17$ |
| A 1651 [a] | 0.084 | pro | $0.31 \pm 0.16$ | $12 \pm 7$ | $0.37 \pm 0.19$ |
| A 401 | 0.074 | pro | $0.46 \pm 0.08$ | $25 \pm 6$ | $0.60 \pm 0.10$ |
| A 399 | 0.072 | obl | $0.50 \pm 0.14$ | $38 \pm 5$ | $0.58 \pm 0.04$ |
| A 2256 | 0.058 | pro | $0.54 \pm 0.14$ | $34 \pm 14$ | $0.72 \pm 0.11$ |
| A 1656 | 0.023 | pro | $0.70 \pm 0.28$ | $33 \pm 30$ | $0.81 \pm 0.21$ |

NOTE. — For ambiguous clusters, both prolate and oblate solutions are listed. $z$ is the redshift, $q_{\rm int}$ (ellips.) the cluster maximum axis ratio under an ellipsoidal assumption, $i$ the inclination angle, $q_{\rm int}$ (triax.) the cluster maximum axis ratio under a triaxial assumption.

[a]Cooling flow clusters.

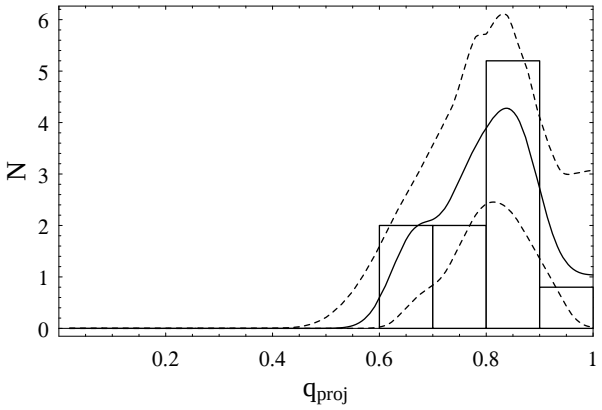


FIG. 1.— Normalized distribution of apparent axial ratios. Solid and dashed lines show the non-parametric kernel estimate and the 2-$\sigma$ confidence range using a bootstrap procedure.

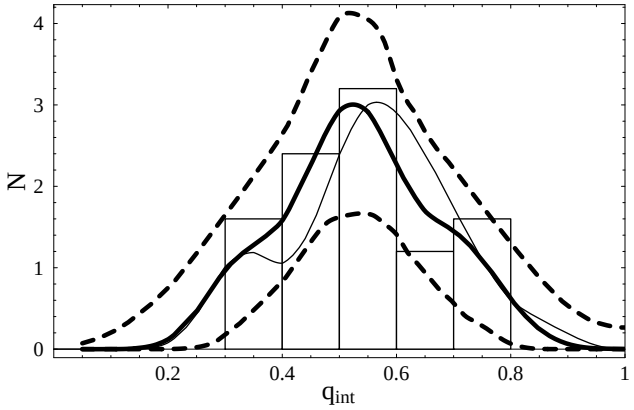


FIG. 2.— Distribution of intrinsic axial ratios. Histogram and thick lines are computed assuming a prolate solution for all ambiguous clusters. Thick-solid and thick-dashed lines show the non-parametric kernel estimate and the 2-$\sigma$ confidence range using a bootstrap procedure. The thin line is the kernel parametric estimate assuming the oblate solution for all ambiguous clusters. Histogram and all distributions are normalized to unity.

In Paper I, the approach used to calculate the elongation along the LOS is discussed in detail; estimated values of $e_{\rm LOS}$ are listed there in Table 4. Once $e_{\rm LOS}$ and $e_{\rm proj}$ are known, both systems Eqs. (8, 9) and Eqs. (10, 11) for prolate and oblate ellipsoids, respectively, can be solved. Given each set of observational constraints, a cluster can admit either only one solution (prolate or oblate) or both. By solving the equation systems, we find that of the 25 clusters in our sample, 15 are compatible only with a prolate morphology, 4 only with an oblate one, while the remaining 6 clusters (hereafter the "ambiguous clusters") are compatible with both the prolate and the oblate assumption. The inferred intrinsic parameters are listed in Table 1. For comparison, in the last column of

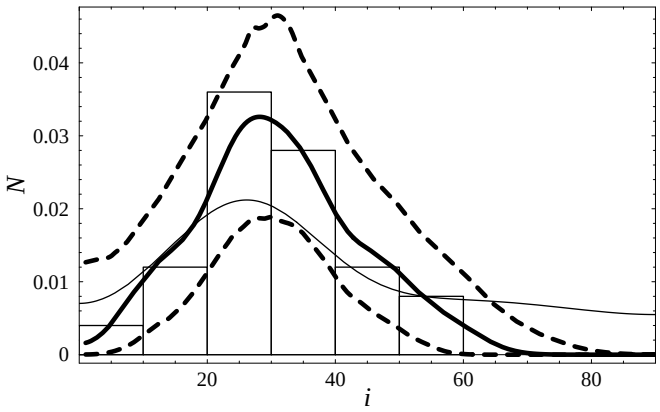


FIG. 3.— Distribution of inclination angles. Histogram and lines are the same as in Fig. 2

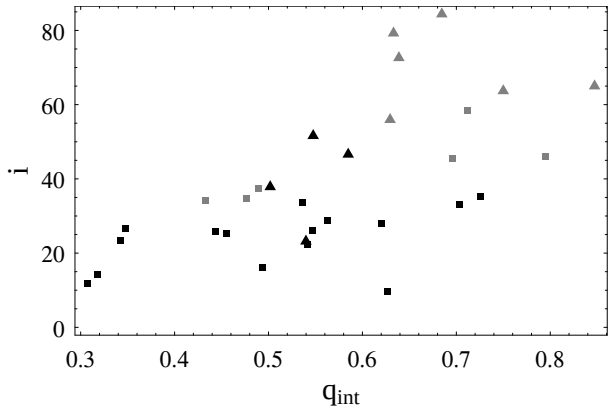


FIG. 4.— Orientation angle versus the intrinsic ellipticity for all clusters in our sample. Boxes and triangles represent prolate and oblate clusters, respectively. Both solutions for ambiguous clusters are plotted in gray.

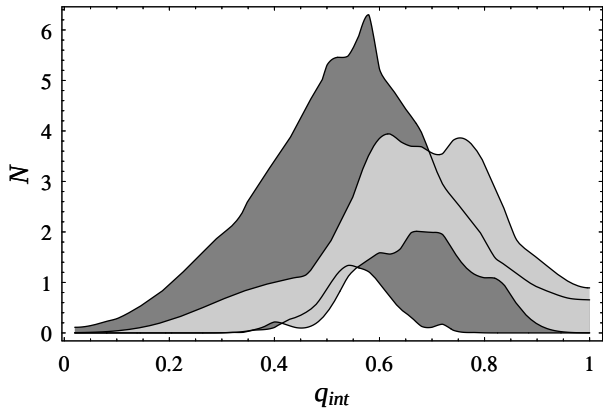


FIG. 5.— 3-$\sigma$ confidence bands of the intrinsic axis ratio distribution, as determined through combined X-ray and SZE measurements with the assumption of an inclined ellipsoidal morphology (dark shaded region, Case I), and as determined under the assumption of triaxial morphology aligned along the LOS (light shaded region). Confidence bands are found by bootstrap resampling.

Table 1 we list the values of $q_{\rm int}$ as computed in Paper I assuming clusters as triaxial structures with null inclination.

To analyze the inferred distribution and to model it with the kernel estimator, we first assume that all of the ambiguous clusters are prolate (Case I) and then that they are all oblate (Case II). These are both extreme cases, but the intrinsic distribution turns out not to be very sensitive to this assumption. In Fig. 2 we plot the distribution of the intrinsic axial ratios. Also in this case, confidence ranges have been determined using the bootstrap procedure with $10^3$ resamplings. It can be seen that the kernel estimate does not change significantly if all ambiguous clusters are assumed to be all prolate or oblate (solid thick and thin line, respectively). The distribution obtained in Case II (thin line) is well within the 2-$\sigma$ confidence level of the one obtained in Case I (thick-dashed lines). In Case I (II), the mean intrinsic axial ratio is $0.54\pm0.03$ ($0.56\pm0.03$), while the median is 0.54 (0.56).

### 3.2. *Inclination angles*

The polar axis of clusters is usually assumed to be randomly oriented with respect to the line of sight. Under this assumption a fraction $\sin i\ di$ of all clusters would have their symmetry axes directed within $di$ of angle $i$ with respect to the line of sight (Binney & Merrifield 1998). The mean value of such a distribution would be $\langle i\rangle_{\rm random} \sim 57^{\circ}$. We instead observe a slightly different picture. The measured distribution of the inclination angles is shown in Fig. 3. The mean inclination angle is $32\pm3$ deg ($37\pm4$ deg) for Case I (II), whereas the median is 29 deg for both cases. Observed clusters show an excess of clusters with their polar axes closely aligned with the line of sight, and a strong deficit of clusters with high values of $i$. The distribution plotted in Fig. 3 has been obtained without considering the error $\Delta i$ when calculating the kernel widths. Using $h_i^{'}$ instead of $h_i$ causes a further broadening of the distribution; both the excess of small values of $i$ and the discrepancy with the assumption of a random distribution still hold.

Fig. 4 shows a plot of the orientation angle versus the intrinsic ellipticity for all clusters in our sample. The most elongated clusters (small values of $q_{\rm int}$) turn out to be prolate nearly aligned with the line of sight. This is most probably due to a bias in the selection of the clusters in the sample. Clusters with low X-ray luminosity, which are stretched along the line of sight are preferentially included in a surface brightness limited survey. Both the ellipticity and the inclination inferred for ambiguous clusters are quite sensitive to the assumed shape. The oblate solution implies a more spherical geometry (larger values of $q_{\rm int}$) and a more inclined polar axis than does the prolate solution. In fact, ambiguous clusters can have inclination angles $\gtrsim 60$ deg only if they are oblate.

### 3.3. *Rotational versus triaxial spheroids*

While in Paper I we assumed galaxy clusters to be triaxial ellipsoids aligned along the LOS, in this paper we have relaxed the assumption of the null inclination, allowing clusters to be inclined along the LOS, but we have put a slightly tighter constraint on their morphology, forcing them to be ellipsoids of revolution.

We observe a tight concordance between the results obtained in the two analyses. Estimated values of $q_{\rm int}$ computed under the two assumptions are in agreement in most cases (see Table 1). The case of a cluster compatible only with the prolate (oblate) shape corresponds to a triaxial cluster with the major (minor) axis oriented along the line of sight. Ambiguous clusters correspond to triaxial shapes having the middle axis directed along the line of sight. The two distributions of the intrinsic axis ratio as obtained either in the present analysis or in Paper I are represented in Fig. 5 (dark and light shaded regions, respectively). As a general trend, we observe that

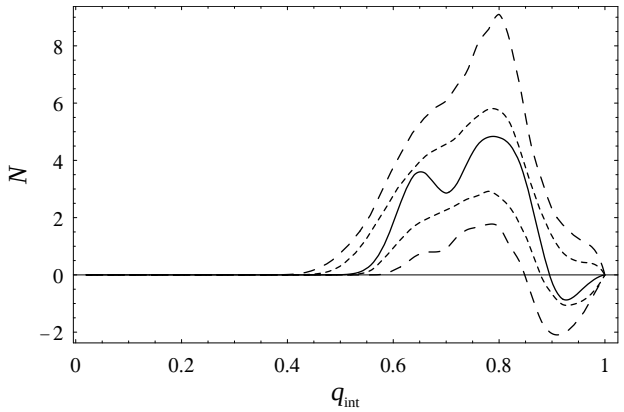


FIG. 6.— Deprojected distribution of intrinsic axis ratios assuming that all clusters are randomly oriented prolate spheroids (solid line). Short-dashed and long-dashed lines show the 1 and 2-$\sigma$ confidence limits, respectively, estimated using a bootstrap re-sampling technique.

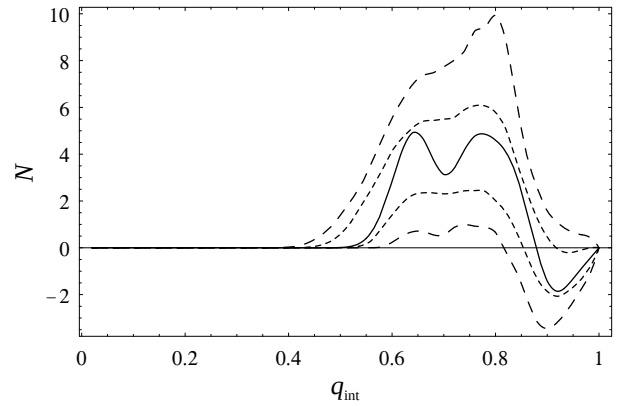


FIG. 7.— Deprojected distribution of intrinsic axial ratios assuming that all clusters are randomly oriented oblate spheroids (solid line). Short-dashed and long-dashed lines show the 1 and 2-$\sigma$ confidence limits, respectively, estimated using a bootstrap re-sampling technique.

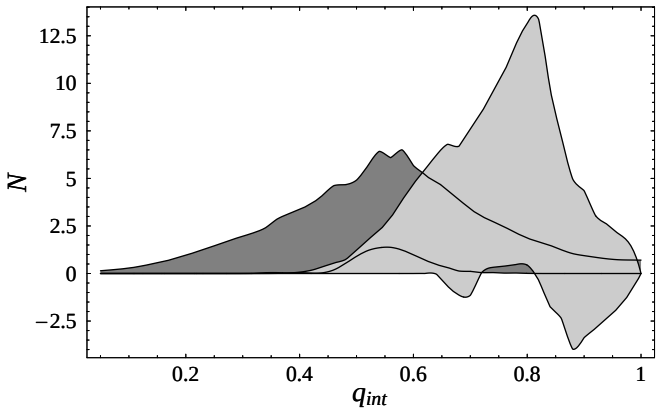


FIG. 8.— 3-$\sigma$ confidence bands of the intrinsic axial ratios, as determined from combined X-ray and SZE measurements (dark shaded region), and of the deprojected distribution of observed axial ratios, assuming that clusters are randomly oriented prolate spheroids (light shaded region). Confidence bands are found by bootstrap re-sampling.

galaxy clusters turn out to be slightly more elongated when modelled as ellipsoids of revolution than in the case of triaxial ellipsoids (showing an average ratio of the minor to the major axis of $\sim 0.63\pm0.03$). This effect is due to the capability of triaxial shapes to fit observed data without the need of extreme axis ratios.

## 4. DEPROJECTED DISTRIBUTION

In this section, we compute the distribution of the intrinsic axis ratio with a third method. The observed projected axial ratio distribution, $\hat{f}(q_{\rm proj})$, can in fact be inverted under appropriate assumptions in order to obtain the intrinsic distribution of the axis ratios. If clusters were all randomly oriented prolate ellipsoids, the intrinsic distribution $\hat{N}_{\rm Pro}$ could be written as (Ryden 1996)

$$\hat{N}_{\rm Pro}(q_{\rm int}) = \frac{2\sqrt{1-q_{\rm int}^2}}{\pi q_{\rm int}} \int_0^{q_{\rm int}} \frac{d}{dq}\left(q^2 \hat{f}(q)\right) \frac{dq}{\sqrt{q_{\rm int}^2 - q^2}}. \quad (16)$$

If, on the contrary, all systems are assumed to be randomly oriented oblate ellipsoids, then the intrinsic distribution can be written as:

$$\hat{N}_{\rm Obl}(q_{\rm int}) = \frac{2q_{\rm int}\sqrt{1-q_{\rm int}^2}}{\pi} \int_0^{q_{\rm int}} \frac{d}{dq}\left(\frac{\hat{f}(q)}{q}\right) \frac{dq}{\sqrt{q_{\rm int}^2 - q^2}}. \quad (17)$$

To take into account the effect of the finite sample size, confidence levels for $\hat{N}_{\rm Pro}$ and $\hat{N}_{\rm Obl}$ have been derived using a bootstrap re-sampling procedure, see § 3. The bootstrap estimates of $\hat{f}$ are then inverted to compute estimates of the intrinsic distributions $\hat{N}_{\rm Pro}$ and $\hat{N}_{\rm Obl}$. Confidence intervals are assigned to each value of $q_{\rm int}$ by finding values of $\hat{N}_{\rm Pro}$ and $\hat{N}_{\rm Obl}$ that lie above (below) some upper (lower) confidence limits. Accurate confidence limits were built using $10^3$ bootstrap re-samplings. The resulting intrinsic axial ratio distributions are plotted in Figs. 6 and 7; these were obtained assuming purely prolate and oblate morphologies, respectively. Negative values in the inverted distributions are evidence against the underlying hypotheses (Ryden 1996; Cooray 2000). The assumption that all clusters are randomly oriented prolate ellipsoids turns out to be consistent with the observed distribution of projected axial ratios, see Fig. 6. On the other hand the hypothesis that all clusters are purely oblate is discarded at the 1-$\sigma$ confidence limit since the resulting intrinsic distribution is negative for high values of $q_{\rm int}$, see Fig. 7. However, at the 2-$\sigma$ confidence level, such an hypothesis cannot be rejected, given the observed ellipticities of our sample clusters.

We now compare the intrinsic distributions of axis ratios obtained using our deprojection technique through X-ray and SZE observations, with the above inverted distribution. We have taken into account the 3-$\sigma$ confidence levels of the intrinsic axis ratio distribution obtained with combined X-ray/SZE method, estimated independently for Case I and II in § 3. We have then obtained the concordance region by holding all points compatible with at least one of the cases. The resulting region is plotted in Fig. 8 in dark gray. The light gray region shows the inverted distribution of observed axial ratios, assuming that clusters are randomly oriented prolate spheroids. With respect to our X-ray/SZE technique, the deprojection method leads to a deficit of nearly spherical structures (low values of $q_{\rm int}$) and to an overabundance of highly elongated clusters. The same discrepancy is observed if the distribu-

tion of observed axial ratios is inverted assuming that clusters are randomly oriented oblate spheroids. Both assumptions that clusters are either all randomly oriented prolate or oblate spheroids do not provide suitable explanation for the intrinsic distribution of our sample.

## 5. GRAVITATIONAL LENSING CONSTRAINTS

As already discussed in Paper I, a third independent observational input can both break the degeneracy between oblate and prolate models and determine cosmological parameters. Such an input can be provided by observations of strong lensing events. Whereas the ICM distribution traces the gravitational potential, gravitational lensing directly maps the cluster total mass. We remark that since we are dealing with an ellipsoidal ICM distribution, the isodensity contours will not in general be ellipsoidal, this being approximately true only for a small value of the ellipticity (Fox & Pen 2002). Observations of strong lensing events can put accurate constraints on the convergence, i.e. the dimensionless projected surface density of the total mass distribution of the lens. Assuming hydrostatic equilibrium and a $\beta$-model for the ICM, the central value of the convergence reads (De Filippis et al. 2005, Eq. (C7)) :

$$k_0 = \frac{3\pi\beta k_{\rm B} T_{\rm e}}{c^2} \frac{D_{\rm cs}}{D_{\rm s}} \frac{1}{\theta_{\rm c,proj}} \left(1+e^2_{\rm proj}\right) \times \begin{cases} \dfrac{e_{\rm int}}{e^2_{\rm proj}} & \text{if prolate} \\ \dfrac{e^2_{\rm proj}}{e_{\rm int}} & \text{if oblate} \end{cases} \tag{18}$$

where $D_{\rm cs}$ and $D_{\rm s}$ are the angular diameter distances from the deflecting cluster to the lensed background source and from the observer to the source, respectively.

The equation for the convergence can be coupled to those discussed in § 2 to determine if the cluster is oblate or prolate, and to estimate one cosmological parameter, in particular $H_0$, together with the shape parameters $i$ and $e_{\rm int}$. Additional multiple image systems allow us to estimate further cosmological parameters (see Paper I).

## 6. SYSTEMATICS

Several systematic uncertainties that depend on the physical state of the ICM could affect our determination of the intrinsic structure of a galaxy cluster. Let us review some effects.

### 6.1. *Cooling flows and temperature gradients*

Departures from isothermality such as a non constant temperature profile or temperature sub-structures mainly affect our analysis through the SZE, since $\Delta T \propto \int n_{\rm e} T dl$.

ICM temperature profiles have been accurately measured thanks to new generation X-ray satellites for several nearby relaxed clusters (Piffaretti et al. 2005; Vikhlinin et al. 2005b), although, due to restricted field of view or background levels, in most cases such measurements are only possible out to one-third/half of the virial radius. Results are still controversial, but some recent investigations seemed to find a similar behaviour in the ICM temperature distribution, with a broad peak followed by a decrease at larger radii (Piffaretti et al. 2005; Vikhlinin et al. 2005a). Cooling processes also alter the temperature profiles with sharp drops within cluster cores (Allen et al. 2001). Similar measurements for large samples of more distant clusters are instead still lacking.

Since the SZE depends essentially on the pressure profile of the cluster, the presence of a cooling flow can affect our estimate of the cluster extent along the line of sight. Our assumption of isothermality in the X-ray analysis generally leads to an overestimate of the temperature and (to a lesser extent) the pressure in the cool region. This in turn leads to an overestimate of the expected SZE signal. The observed temperature decrement is thus misinterpreted, leading to an underestimate of the LOS extent.

A refined view of cooling processes should account for changes in density profiles as well as the temperature profile, with the effect due to decrease of gas temperature moderated by the sudden increase of the gas density. Previous studies addressed the effect of departures from isothermality when using SZE along with X-ray observations. Given our different approach, we interpret as an over (under)-estimation of the LOS elongation what has been previously seen as an under (over)-estimation of the Hubble constant. Based on theoretical models for radiative cooling, it was found that, even after excluding $\sim 80\%$ of the cooling-flow region, an error of $\sim 10\%$ on the elongation could affect analyses restricted to radii of $1.5\, r_{\rm c}$ (Majumdar & Nath 2000).

In order to check how much the presence of a central cooling region can affect our analysis, we re-analyzed three massive cooling flow clusters in our sample (RX J1347.5-1145, A 1835 and A 478) using the most recent *Chandra* observations available. We performed morphological and spectral analyses both using the whole cluster extent and excluding the central cool region. Details on the data reduction and on the morphological analysis are given in Paper I. Removing the central region leads to an increase of both values of $\theta_{\rm c}$ ($\approx 60\%$) and $\beta$ ($\gtrsim 6\%$), when fitting a $\beta$-model to the cluster surface brightness elliptical profile. Estimates of central amplitude are strongly affected too. Average isothermal spectral temperatures are larger by $\sim 20\%$ respect to when the values are averaged over the whole cluster extent. The above effects leads to an underestimation of the cluster elongation along the line of sight of $\sim 15\%$, in agreement with previous estimates (Inagaki et al. 1995; Majumdar & Nath 2000).

The effect of a central decrement is opposite to that of a negative gradient at large radii in the temperature profile when determining the cluster structure assuming isothermality (Inagaki et al. 1995; Yoshikawa et al. 1998). If the gas temperature in the outer region is lower than that in the inner region, an overestimation of the LOS extent as large as $\sim 20\%$ is possible (Inagaki et al. 1995).

Actually, systematic errors due to departures from isothermality are overwhelmed by large observational uncertainties in both the actual temperature profile and the SZE measurement. Results turn out to be quite insensitive to details of the gas modelling and the isothermal $\beta$-model can still provide a reasonably accurate model (Bonamente et al. 2005). Effects due to either central drops or temperature gradients at large radii could partially compensate each other and could be combined in a systematic deviation as large as $15\%$, whose sign depends on which effect prevails.

### 6.2. *Density clumping*

Small-scale density fluctuations on X-ray measurements arising from accretion events and major mergers could introduce a further bias. Clumping in the gas density distribution causes an enhancement of the X-ray brightness by a factor $C_{\rm n} = \langle n_{\rm e}^2 \rangle / \langle n_{\rm e} \rangle^2$ with respect to a uniform smooth atmosphere, while SZE measurements are not affected. This leads to an underestimate of the elongation along the line of sight for $C_{\rm n} > 1$ ($e_{\rm LOS} \propto C_{\rm n}^{-1}$) .

Currently, there is no observational evidence of significant clumping in galaxy clusters (Reese et al. 2002), al-

though numerical hydro-simulations show that $C_{\rm n} \simeq 1.34$ (Mathiesen et al. 1999). More detailed simulations and observations are required to estimate the extent and the effect that clumpiness could induce on our analysis.

### 6.3. *Overall departure*

In general, systematic effects do not act all in the same direction and require a very detailed modelling in order to correct for an amount that might be not very significant. Different effects can combine to give a nearly null bias, as suggested from analysis of subsamples. In particular, cooling flow clusters in our sample are equally split between those elongated and compressed along the LOS, suggesting that including a temperature profile or other effects would not drastically change the results on their average structure.

Departures from an isothermal ICM in hydrostatic equilibrium should not introduce serious errors. The reliability of isothermal models to predict expected X-ray or SZE observations was tested against high-resolution, hydrodynamic cluster simulations (Flores et al. 2005). As long as one focuses on cluster regions that are less sensitive to recent mergers, assuming isothermal gas allows accurate X-ray estimations even if the gas has a strong temperature gradient. SZE decrement maps can also be accounted for although not as successfully as for the X-ray case (Flores et al. 2005).

## 7. DISCUSSION AND CONCLUSIONS

We have studied the intrinsic structure of clusters of galaxies by combining X-ray and SZE observations and modelling them as ellipsoids of revolution. We find that clusters of galaxies cannot be described as a population of either purely oblate or purely prolate spheroids with a random inclination of the symmetry axis respect to the LOS. A mixed population is instead required to model the data, prolate-like shapes being slightly preferred.

We have then compared our results with what is expected from a population of randomly oriented galaxy clusters, having the observed projected ellipticities of our sample. In contrast with the intrinsic population expected under this hypothesis, we find a significant excess of clusters nearly aligned along the line of sight. Furthermore, high inclinations angles are observed mainly for oblate clusters, while most elongated clusters turn out to be only prolate. If we believe the hypothesis of randomly oriented polar axes to be correct, the behavior of the clusters in our sample could be explained by a combination of two effects: a first one caused by selection effects, which favours the detection of clusters more elongated along the line of sight, and a second one due to the fact that an oblate or prolate ellipsoidal model might not be correct for galaxy clusters, and a more general triaxial morphology should instead be used. Even though clusters in our sample were originally selected according to their luminosity with a selection threshold well above the detection limit, a selection bias on the basis of X-ray surface brightness can still persists for extremely elongated clusters. The second effect would instead lead to more dramatic conclusions.

Higher accuracy measurements and a better understanding of systematics are needed to confirm our results. Although approximating galaxy clusters as isothermal systems in hydrostatic equilibrium with ellipsoidal matter distributions can be quite simplistic for some clusters, it can give a first insight on their intrinsic structure. Some numerical simulations also seem to support this view (Flores et al. 2005). A natural development could be using more sophisticated models than the isothermal-$\beta$ profile to describe the ICM. Due to the infinite extent assumed in this model, the slope of the surface brightness distribution at large radii could be too shallow and might miss a progressive steepening with radius. Unfortunately, data of sufficient quality are often missing too and ICM can be traced with sufficient accuracy only up to few core radii. Furthermore, the $\beta$-model provide a very good framework for the gas density distribution of most of the observed clusters in our sample and still provide a bench-mark for comparison in a statistical sample. High-resolution spatially resolved spectral measurements of temperature profile are restricted within the very inner regions for most of the clusters and some extrapolation technique, with a degree of unavoidable liberty, is therefore required (Schmidt et al. 2004). Furthermore, from recent studies there appeared to be little difference in the accuracy of the mass estimation from X-ray or SZE measurements whether using isothermal or general, numerically or observationally motivated, temperature profile methods (Hallman et al. 2005). While waiting for more precise measurements on a cluster-by-cluster basis, using only a few numbers, i.e. a single temperature, a constant axial ratio and a simple model for the ICM distribution, is still a conservative approach. A crucial step to strengthen the statistical significance of our analysis would be the use of an unbiased and larger sample. The sample we have been considering in this paper is restricted to X-ray selected clusters for which a SZE analysis had been already reported. Preferential inclusion of high-S/N clusters could bias the sample towards clusters highly elongated towards the LOS.

The problem of determining the intrinsic shape of galaxy clusters could be in principle completely solved for quite general morphologies, but uncertainties on observed quantities make this task still hard to obtain. An improved accuracy in the measurement of the SZE would also allow to look for trends in the intrinsic structure with mass or redshift as shown by numerical simulations (Jing & Suto 2002; Kasun & Evrard 2005; Paz et al. 2006). Unfortunately, present data are not sufficiently precise to test such predicted correlations (De Filippis et al. 2005). As we have discussed in Paper I, a proper triaxial structure is well suited to fit observations. Additional independent constraints from gravitational lensing observations can break the degeneracy on the intrinsic shape of galaxy clusters and discriminate between triaxial spheroids and ellipsoids of revolution. In view of future progresses on the observational side, a more accurate adaptation of our method, in which both the assumptions of isothermality and of a density profile approximated by a $\beta$-model are abandoned, will be presented in a forthcoming paper. Our complete 3-D deprojection method will also be investigated with numerical simulations. The comparison of the projected properties of 3-D simulated haloes with observational data could help to understand the intrinsic structure and to test the approximations and hypotheses used (Paz et al. 2006). With respect to similar previous analyses of groups based on the optical distribution of member galaxies, our method would have the advantage to be not affected by systematics due to finite sampling (Paz et al. 2006).

The authors thank the referee for the useful suggestions. This work has been partially supported by MIUR grant COFIN 2004020323 and by NASA grants NAS8-39073 and NAS8-00128. M.S. is supported by the Swiss National Science Foundation and by the Tomalla Foundation. This re-

search has made use of NASA's Astrophysics Data system Bibliographic Services.

## APPENDIX

## TWO-DIMENSIONAL PROJECTION OF A THREE-DIMENSIONAL ELLIPSOID

The expressions reported in Sections 2 and 5 can be obtained from the results in Paper I. Let us denote the observer coordinate system as $\{x_{i,\rm obs}\}$, $i = 1, 2, 3$. The polar axis forms an angle $i$ with the line of sight, $x_{3,\rm obs}$. We assume that the major axis of the projected ellipses always lies along the $x_{1,\rm obs}$-axis, i.e. the polar axis lies in the $x_{1,\rm obs} - x_{3,\rm obs}$ plane in the prolate case and in the $x_{2,\rm obs} - x_{3,\rm obs}$ plane in the oblate case. As an example, in the prolate case, the relation between the two coordinate systems are

$$x_{1,\rm int} = x_{1,\rm obs} \cos i + x_{3,\rm obs} \sin i, \tag{A1}$$

$$x_{2,\rm int} = x_{2,\rm obs}, \tag{A2}$$

$$x_{3,\rm int} = x_{3,\rm obs} \cos i - x_{1,\rm obs} \sin i. \tag{A3}$$

Following the notation in Paper I, for a prolate ellipsoid $v_1 = v_2 = e_{\rm int}$, $\theta_{c3} = \theta_c$; for an oblate ellipsoid $v_1 = v_2 = 1/e_{\rm int}$, $\theta_{c3} = \theta_c/e_{\rm int}$. The observed core radius is

$$\theta_{\rm proj} = \theta_c \times \begin{cases} \dfrac{e_{\rm proj}}{e_{\rm int}} & \text{prolate case} \\ 1 & \text{oblate case} \end{cases} \tag{A4}$$

Substituting in the formulae reported in Paper I, we obtain the expressions used in Sections 2 and 5.

## REFERENCES


Alam, S. M. K., & Ryden, B. S. 2002, ApJ, 570, 610
Allen, S. W., Schmidt, R. W., & Fabian, A. C. 2001, MNRAS, 328, L37
Basilakos, S., Plionis, M., & Maddox, S. J. 2000, MNRAS, 316, 779
Bertola, F., & Capaccioli, M. 1975, ApJ, 200, 439
Binggeli, B. 1980, A&A, 82, 289
Binney, J., & de Vaucouleurs, G. 1981, MNRAS, 194, 679
Binney, J., & Merrifield, M. 1998, Galactic astronomy (Princeton: Princeton University Press)
Bonamente, M., Joy, M., LaRoque, S. J., Carlstrom, J. E., Reese, E. D., & Dawson, K. S. 2005, astro-ph/0512349
Carter, D., & Metcalfe, N. 1980, MNRAS, 191, 325
Cooray, A. R. 1998, A&A, 333, L71
—. 2000, MNRAS, 313, 783
D'Agostini, G. 2004, physics/0403086
De Filippis, E., Sereno, M., Bautz, M. W., & Longo, G. 2005, ApJ, in press; astro-ph/0502153
de Theije, P. A. M., Katgert, P., & van Kampen, E. 1995, MNRAS, 273, 30
Donahue, M., Gaskin, J. A., Patel, S. K., Joy, M., Clowe, D., & Hughes, J. P. 2003, ApJ, 598, 190
Fabricant, D., Rybicki, G., & Gorenstein, P. 1984, ApJ, 286, 186
Fasano, G., & Vio, R. 1991, MNRAS, 249, 629
Fixsen, D. J., Cheng, E. S., Gales, J. M., Mather, J. C., Shafer, R. A., & Wright, E. L. 1996, ApJ, 473, 576
Flores, R. A., Allgood, B., Kravtsov, A. V., Primack, J. R., Buote, D. A., & Bullock, J. S. 2005, ArXiv Astrophysics e-prints
Fox, D. C., & Pen, U. 2002, ApJ, 574, 38
Hallman, E. J., Motl, P. M., Burns, J. O., & Norman, M. L. 2005, astro-ph/0509460
Hubble, E. P. 1926, ApJ, 64, 321
Illingworth, G. 1977, ApJ, 218, L43
Inagaki, Y., Suginohara, T., & Suto, Y. 1995, PASJ, 47, 411
Jing, Y. P., & Suto, Y. 2002, ApJ, 574, 538
Kasun, S. F., & Evrard, A. E. 2005, ApJ, 629, 781
Kazantzidis, S., Kravtsov, A. V., Zentner, A. R., Allgood, B., Nagai, D., & Moore, B. 2004, ApJ, 611, L73
Majumdar, S., & Nath, B. B. 2000, ApJ, 542, 597
Mason, B. S., Myers, S. T., & Readhead, A. C. S. 2001, ApJ, 555, L11
Mathiesen, B., Evrard, A. E., & Mohr, J. J. 1999, ApJ, 520, L21
Mohr, J. J., Evrard, A. E., Fabricant, D. G., & Geller, M. J. 1995, ApJ, 447, 8
Noerdlinger, P. D. 1979, ApJ, 234, 802
Paz, D. J., Lambas, D. G., Padilla, N., & Merchán, M. 2006, MNRAS in press, astro-ph/0509062
Piffaretti, R., Jetzer, P., Kaastra, J. S., & Tamura, T. 2005, åp, 433, 101
Plionis, M., Barrow, J. D., & Frenk, C. S. 1991, MNRAS, 249, 662
Plionis, M., Basilakos, S., & Tovmassian, H. M. 2004, MNRAS, 352, 1323
Reblinsky, K. 2000, A&A, 364, 377
Reese, E. D., Carlstrom, J. E., Joy, M., Mohr, J. J., Grego, L., & Holzapfel, W. L. 2002, ApJ, 581, 53
Ryden, B. 1992, ApJ, 396, 445
Ryden, B. S. 1996, ApJ, 461, 146
Schmidt, R. W., Allen, S. W., & Fabian, A. C. 2004, MNRAS, 352, 1413
Sereno, M., Covone, G., Piedipalumbo, E., & de Ritis, R. 2001, MNRAS, 327, 517
Tegmark, M., Strauss, M. A., Blanton, M. R., Abazajian, K., Dodelson, S., Sandvik, H., Wang, X., & Weinberg, D. H. e. a. 2004, Phys. Rev. D, 69, 103501
Thakur, P., & Chakraborty, D. K. 2001, MNRAS, 328, 330
Vikhlinin, A., Kravtsov, A., Forman, W., Jones, C., Markevitch, M., Murray, S. S., & Van Speybroeck, L. 2005a, ArXiv Astrophysics e-prints
Vikhlinin, A., Markevitch, M., Murray, S. S., Jones, C., Forman, W., & Van Speybroeck, L. 2005b, ApJ, 628, 655
Vio, R., Fasano, G., Lazzarin, M., & Lessi, O. 1994, A&A, 289, 640
Wang, L., Caldwell, R. R., Ostriker, J. P., & Steinhardt, P. J. 2000, ApJ, 530, 17
Wang, Y.-G., & Fan, Z.-H. 2004, ApJ, 617, 847
West, M. J. 1994, MNRAS, 268, 79
Yoshikawa, K., Itoh, M., & Suto, Y. 1998, PASJ, 50, 203
Zaroubi, S., Squires, G., de Gasperis, G., Evrard, A. E., Hoffman, Y., & Silk, J. 2001, ApJ, 561, 600
Zaroubi, S., Squires, G., Hoffman, Y., & Silk, J. 1998, ApJ, 500, L87